MICROBIOLOGY

Direct single-cell observation of a key *Escherichia coli* cell-cycle oscillator

Ilaria Iuliani[1,2,3]†, Gladys Mbemba[1], Marco Cosentino Lagomarsino[3,4]*‡, Bianca Sclavi[2]*‡

Initiation of DNA replication in *Escherichia coli* is coupled to cell size via the DnaA protein, whose activity is dependent on its nucleotide-bound state. However, the oscillations in DnaA activity have never been observed at the single-cell level. By measuring the volume-specific production rate of a reporter protein under control of a DnaA-regulated promoter, we could distinguish two distinct cell-cycle oscillators. The first, driven by both DnaA activity and SeqA repression, shows a causal relationship with cell size and divisions, similarly to initiation events. The second one, a reporter of DnaA activity alone, loses the synchrony and causality properties. Our results show that transient inhibition of gene expression by SeqA keeps the oscillation of volume-sensing DnaA activity in phase with the subsequent division event and suggest that DnaA activity peaks do not correspond directly to initiation events.

INTRODUCTION

The DnaA protein is a key factor for the initiation of DNA replication and an essential protein for most known bacteria (*1*). When it is in its adenosine triphosphate (ATP)–bound ("active") form, DnaA binds to a set of specific sites at the origin of DNA replication (oriC) leading to the formation of an oligomeric structure and the subsequent melting of an AT-rich region required for the assembly of the DNA replication forks (*2*–*5*). On the basis of experiments where the expression of DnaA is artificially controlled, it is believed that the amount of DnaA-ATP needs to reach a threshold value once per cell cycle for this structure to form, leading to the initiation of DNA replication (*6*–*8*).

Experiments in bulk exploring a large range of growth rates have shown that cell size at initiation of DNA replication is related to the growth rate and is correlated with the concentration of the DnaA protein (*9*). In *Escherichia coli*, the DnaA-dependent regulatory circuit is made of different positive and negative components (*10*, *11*). Several factors contribute to the decrease in DnaA activity after initiation has taken place (*12*). First, the expression of the *dnaA* gene is prevented for a fraction of the cell cycle by the SeqA protein binding to hemimethylated GATC sites at the promoter and within the *dnaA* gene itself, after their replication (*13*–*17*). The *dnaA* gene is located close to the replication origin, and SeqA follows the forks, transiently repressing its expression immediately after each initiation. Second, inhibition of transcription initiation by the oligomerization of DnaA-ATP itself decreases the production of DnaA (*18*–*21*). Both of these processes inhibit DnaA protein expression and are related to the timing of initiation of DNA replication and to fork progression through the genomic position of its gene (*14*). After initiation has taken place, the rate of hydrolysis of the ATP bound to DnaA is increased via an interaction with the Hda protein mediated by the β-clamp during ongoing DNA replication in a process called RIDA (regulatory inactivation of DnaA) (*22*). Last, the binding of DnaA-ATP to the *datA* site also contributes to the conversion of DnaA-ATP to DnaA–adenosine diphosphate (ADP) after initiation, via *datA*-dependent DnaA-ATP hydrolysis (*23*). The increase in DnaA-ATP required for the initiation of a new DNA replication cycle depends on the timely accumulation of newly expressed protein (*7*, *8*, *14*) and on the binding of DnaA to the DARS1 and DARS2 sites, contributing to a further increase in the DnaA-ATP to DnaA-ADP ratio by favoring the exchange of the DnaA-bound nucleotide (*10*, *24*–*26*).

Together, these processes lead to the belief that DnaA activity is a cell-cycle oscillator coupled to cell size (*27*). However, given the complexity of this regulatory circuit, one of the major challenges in the field has been to find a way to measure the oscillations in DnaA activity in real time, particularly because they need to be observed at the level of the single cell due to the difficulties in synchronizing the cell cycle of *E. coli* cells. Moreover, while the different mechanisms regulating DnaA activity via ATP hydrolysis have been carefully characterized, less is known on the real-time dynamics of DnaA's gene expression as a function of the cell cycle and its coupling to cell size. Here, we rely on a chromosomal promoter-reporter system based on the *dnaA* promoter itself as a reporter of the relative contributions of DnaA-ATP and SeqA on the expression of DnaA to measure its relationship with cell size and cell division.

Dynamically monitoring these oscillations in single cells is particularly important because it makes it possible to compare the oscillator with known single-cell observations of replication-initiation reporters (*28*–*35*). These studies reported a constant (independent from cell size at initiation) added size between initiation events and also between the initiation of DNA replication and cell division (*32*). However, a direct link is still missing between possible single-cell oscillations in DnaA activity and cell size correlation patterns of initiation events.

RESULTS

The *dnaA* promoter as a reporter of the changes in DnaA-ATP activity and SeqA in vivo

Because DnaA in the cell exists under two forms, ATP and ADP bound, with only the former being the one that can initiate DNA

[1]LBPA, UMR 8113, CNRS, ENS Paris-Saclay, 91190 Gif-sur-Yvette, France. [2]LCQB, UMR 7238, CNRS, Sorbonne Université, 4 Place Jussieu, 75005 Paris, France. [3]IFOM ETS—The AIRC Institute of Molecular Oncology, Via Adamello 16, 20139 Milan, Italy. [4]Dipartimento di Fisica, Università degli Studi di Milano, and I.N.F.N, Via Celoria 16, 20133 Milan, Italy.
*Corresponding author. Email: marco.cosentino-lagomarsino@ifom.eu (M.C.L.); bianca.sclavi@sorbonne-universite.fr (B.S.)
†Present address: Department of Computational Biology, University of Lausanne and Swiss Institute of Bioinformatics, Lausanne, Switzerland.
‡These authors contributed equally to this work.

replication, we looked for a reporter of DnaA-ATP activity to study the regulation of DNA replication in *E. coli* in real time in vivo. We have chosen to use the role of DnaA as a transcription factor (*36*, *37*) to report on the changes in DnaA activity. One of the best-characterized targets of transcription regulation by DnaA is its own promoter (*19*, *20*). We have constructed a reporter cassette where the fast-folding *mut2-gfp* gene is under control of the *dnaA*P2 promoter sequence (from −136 to +48 relative to the transcription start site). This green fluorescent protein (GFP) is highly soluble and stable (*38*). To obtain an effect of SeqA and gene dosage on our reporter as similar as possible to the endogenous promoter, we have inserted the *dnaA*P2 promoter reporter cassette in the genome within the Ori macrodomain, at the "Ori3" locus downstream of the *aidB* gene (4,413,507 bp) (*39*), which was used in a previous study (*40*). The coordinate of this site is at 21% of the right replicore, and the replication fork should pass through it on average about 8 min after initiation of DNA replication.

Regulation of expression of the *dnaA* gene depends on a promoter region that includes two promoters, P1 and P2 (*41*). P2 is found downstream of P1 and includes a GC-rich discriminator region overlapping with the transcription start site, making transcription initiation negatively regulated by ppGpp (*42*). P2 is the stronger promoter in exponential phase and is thought to provide the main growth rate–dependent regulation of DnaA expression, while P1 provides a basal level of constitutive expression, similarly to what is found at ribosomal promoter regions (*20*, *42*, *43*).

Expression from P2 is negatively regulated by a high concentration of DnaA-ATP (*19*) and positively regulated by DnaA when its concentration decreases (*20*), making it an effective sensor of DnaA-ATP levels. More specifically, two high-affinity sites for DnaA, Box1 and Box2, are found upstream of the *dnaA*P2 promoter. The binding of DnaA-ATP to these two high-affinity sites activates transcription when DnaA-ATP activity is low. As DnaA-ATP concentration increases, the DnaA bound to Box1 and Box2 becomes the scaffold for the formation of an oligomeric structure that represses transcription by occluding the RNA polymerase binding site (*19*, *20*, *44*). Specific mutations in Box1 and Box2 disrupt the DnaA-binding consensus sequence. These mutants decrease the binding affinity for DnaA and thus result in promoters that are only positively regulated (Box1 mutation) or neither positively nor negatively regulated by DnaA-ATP (Box1-Box2 mutation) (*20*). Last, transcription initiation is inhibited by SeqA binding to five GATC sites, two overlapping with the −10 and −35 sequences of P2 and three closely spaced sites found downstream of the transcription start site. An additional set of mutations ("m3SeqA," Fig. 1A) change the sequence of these three GATC sites. A previous study has shown that the set of these three mutations does not affect the synchrony of initiation of DNA replication, but causes a decrease in growth rate and DNA content in rich media (*45*). The two GATC sites overlapping with the −10 and −35 sequence were left intact in order not to affect the binding of RNA polymerase, but a previous study has shown that they have little effect on repression by SeqA and DNA replication parameters (*46*).

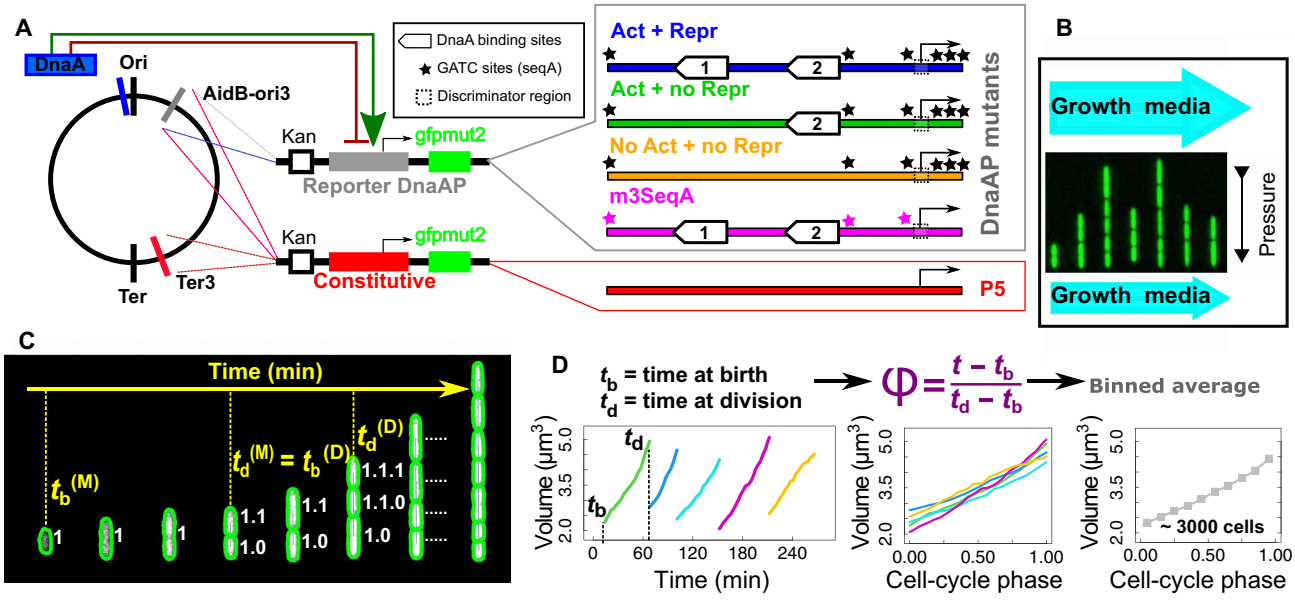

Fig. 1. Robust and long-term single-cell tracking in fast growth conditions. (**A**) We inserted a reporter construct of the *mut2gfp* gene at a specific site downstream of the *aidB* gene in the Ori macrodomain (*39*). Expression of the reporter protein is under control of the native *dnaA*P2 promoter region. A kanamycin resistance cassette is expressed divergently upstream of the promoter. Different promoter mutants with different levels of regulation by DnaA and SeqA were considered. As a reference for baseline gene expression, we used a constitutive promoter (see Methods). (**B**) The experimental device is a two-ended "mother machine" microfluidic channel where growth media flow constantly at the top and bottom of tapered-end micro-channels, ensuring a constant environment (*47*). The picture shows a field of view with seven micro-channels. Differences in flow rates between the two large channels generate a pressure that keeps the bacteria (which can only escape from the larger top end) inside the channels. (**C**) Segmentation/tracking algorithms follow the changes in cell size and fluorescence over time and across generations. The image shows snapshots of the same channel at subsequent times, and $t_{b,d}$ represent the times of birth/division of mother/daughter (M, D) in a lineage. (**D**) To examine the effects of cell-cycle progression, we began by aligning growth and gene expression data with respect to cell-cycle phase (fraction of time spent in the cell cycle), defined as cell-cycle time normalized by the cell's division time.

The effect of the *dnaA*P2 promoter mutations on GFP expression from the chromosomal insertion site has been measured by a plate reader assay and is consistent with the previously published results obtained on a plasmid (*20*) (fig. S1). Mutation of Box1 increases expression relative to the wild-type sequence, while mutation of both Box1 and Box2 decreases expression back to wild-type levels. What is important for this study is that (i) the original promoter ("Act + Repr" in Fig. 1A) senses both DnaA-ATP levels and the transit of the replication forks via the negative effect of SeqA binding, (ii) the promoter stripped of both DnaA binding sites ("no-Act + noRepr" in Fig. 1A) only senses the binding of SeqA, and (iii) the m3SeqA variant without the three GATC sites is only regulated by DnaA-ATP levels.

To achieve single-cell resolution and capture the dynamic changes in cell growth, cell division, and gene expression as a function of the cell cycle as well as across several generations, we used an integrated microfluidics and time-lapse microscopy approach (*47*). In this device, an air pressure–controlled flow system provides a constant environment where cells can grow steadily for several days as the growth medium flows continuously at a constant rate (Fig. 1B).

We studied cells in a fast-growth condition (M9 minimal medium with glucose and casamino acids at 30˚C), where the cells have a mean doubling time of 45 min and initiate DNA replication at two origins. Thousands of single cells were segmented and tracked from movies with frames obtained every 3 min to examine cell cycle–dependent changes in fluorescent protein expression and cell size in lineages comprising up to 15 generations, as described in (*40*) (Fig. 1C).

Table S1 provides a complete list of measured parameters and computed variables. Each experiment yielded 2000-8000 full-cell cycles with a good reproducibility (fig. S2).

As a reference, we considered the expression of the same reporter fluorescent protein under control of a constitutive promoter used in a previous study (*40*). This phage-derived constitutive promoter, "P5," has consensus −10 and −35 sequences and lacks regulation by specific transcription factors; therefore, the GFP production rate in this case can be considered to be largely representative of the change in gene copy number with the passage of the DNA replication fork. To measure its gene expression as a function of the cell cycle, we have inserted the P5-*mut2-gfp* construct at the same origin-proximal locus as the *dnaA*P2-*mut2-gfp* construct (Ori3) as well as at the terminus-proximal locus (Ter3) downstream of the *uspE* gene (see Methods). The results obtained with these strains show that GFP production from an unregulated promoter involves "null" cell cycle–dependent trends due to volume and gene dosage, which, in a regulated promoter, have to be disentangled from any regulatory signal (fig. S3).

Transcription regulation by DnaA-ATP and SeqA causes strong oscillations in volume-specific GFP production rate

We next set out to determine how the expression of GFP under control of the *dnaA*P2 promoter differs from that of a constitutively expressed gene as a function of the cell cycle (Fig. 2, Supplementary Notes, and fig. S3). Crucially, we found that a GFP production rate defined as the discrete time derivative of fluorescence is proportional to cell size (Supplementary Notes and fig. S3). Hence, to see oscillations, we considered volume-specific GFP production. Figure 2 (A to C) and fig. S4 show that strong *dnaA*P2 oscillations emerge compared to unregulated promoters when lineages are aligned by cell-cycle phase. Cell-cycle phase is defined as the fraction of time t/τ spent in the cell cycle, where t is time from birth and τ is interdivision time. This quantity aligns the dynamic data from individual cell cycles as a function of the fractional progression between the times of cell birth and division (*48*). The oscillation pattern is also observed when the data are binned as a function of time to cell division, but not as a function of time from cell birth (Fig. 2, D to F), indicating that the wild-type *dnaA*P2 oscillations are agnostic of cell

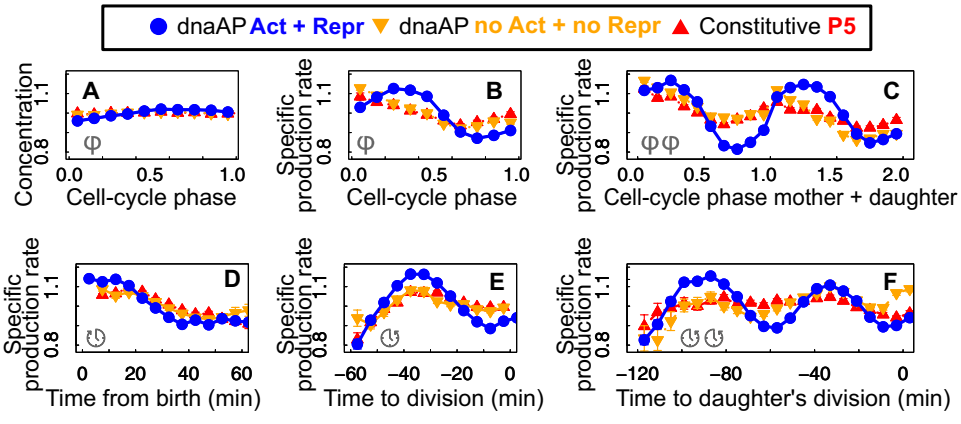

Fig. 2. Regulation of the *dnaA*P2 promoter by DnaA-ATP causes oscillations in GFP production rate beyond the effect of gene dosage. (**A**) Oscillations in GFP concentration as a function of cell-cycle phase are weak for the constitutive promoter (red triangles), the *dnaA*P2 promoter (blue circles), and *dnaA*P2-Box1-Box2, the promoter not regulated by DnaA (orange triangles). (**B**) The fold change in volume-specific GFP production rate from *dnaA*P2 shows a clear peak that is not present for a constitutive promoter or the *dnaA*P2-Box1-Box2 promoter, which follow similar weak trends. (**C**) A sinusoidal oscillation for GFP expression from *dnaA*P2 is observed when taking into account the cell-cycle phase of lineages with two consecutive generations. (**D** and **E**) Volume-specific GFP production rate averaged conditionally to time from birth is very similar for the three promoters, while oscillations are enhanced for the *dnaA*P2 promoter when the same data are averaged conditionally as a function of the time to division. (**F**) Oscillations in GFP expression from *dnaA*P2 are enhanced when averaged conditionally to time to daughter division. If these oscillations correspond to changes in DnaA activity, they are consistent with the model where DNA replication initiating in the mother cell and terminating in the daughter cell will influence the timing of cell division of the daughter (*49*).

birth, and prognostic of the next cell division. Oscillations in GFP expression from *dnaA*P2 are enhanced when averaged conditionally to time to daughter division. If these oscillations correspond to changes in DnaA activity, they are consistent with the model where DNA replication initiating in the mother cell and terminating in the daughter cell will influence the timing of cell division of the daughter (*49*).

Oscillations in *dnaA*P2 promoter activity are a cell size sensor

Given the consensus on the links between cell size and replication initiation, the *dnaA*P2 oscillator can be expected to follow cell size. If that were the case, binning the gene expression data as a function of cell volume should result in an improved synchronization of individual cells' oscillations.

We thus proceeded to test the hypothesis that DnaA activity and/or production rate may be a cell size sensor by binning the data as a function of cell volume. Figure 3 (A and B) shows that volume-binned averages in GFP volume-specific production rate from *dnaA*P2 follow strong oscillations reaching maxima and minima at multiples of a characteristic volume. Notably, in the m3SeqA promoter stripped of SeqA control, the oscillations remain strong but change in timing, volume coupling, and amplitude (Fig. 3C). The same analysis with the data from the constitutive promoter and the mutant *dnaA*P2 promoters also shows oscillations but of smaller amplitude (Fig. 3C).

The underlying oscillation of the constitutive and unregulated *dnaA*P2 promoters reflects increased expression upon the doubling of gene dosage by the passage of the replication fork followed by a decrease as cell size further increases (*48*). Hence, part of these oscillations must be due to dosage effects and dosage-volume correlations, independently from specific regulation by DnaA or SeqA. The dosage-volume correlation is indicative of the strong cell size dependence of initiation of DNA replication.

The effect of the mutation of the DnaA binding sites determines a visible change in amplitude and phase of the average oscillation (when averaged conditionally with respect to cell volume), consistent with a volume-dependent regulation by the concentration of free DnaA-ATP, increasing gene expression rate after the repression by SeqA and the subsequent increase in gene copy number and decreasing it when its concentration is the highest, at around the time of initiation (Fig. 3C). Thus, our data give an unprecedented view of the regulatory effect of the oscillations of DnaA activity in single cells. In the absence of DnaA-dependent regulation (noAct + noRepr), the promoter is only repressed by SeqA. In this case, volume-specific production rate shows a visible change in phase compared to the constitutive promoter (Fig. 3C). On the other hand, mutation of the SeqA sites in the presence of DnaA-dependent regulation shows a visible shift in the volume at which oscillation minima occur compared to the wild-type *dnaA*P2 promoter (Fig. 3C). These results are consistent with repression by SeqA delaying gene expression from the newly replicated promoter (*13*).

To shed more light into the size-sensing properties of the *dnaA*P2 promoter, we performed conditional averages of volume-specific GFP production rate fixing cell volume as well as different additional cell-cycle variables. Specifically, we plotted the usual conditional average of volume-specific GFP production rate versus cell-cycle phase, volume, time to the next division, and time from birth for different groups of cells with similar size at birth (Fig. 4A). The rationale behind these plots is the expectation that the variables that are more directly coupled to the oscillations should be insensitive to variations of any extrinsic variable like size at birth. In particular, if the oscillator is a true volume sensor, it should have no memory of size at birth.

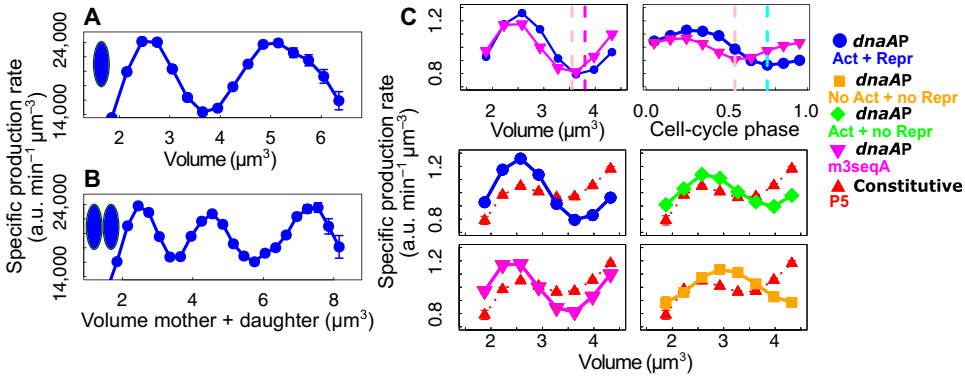

Fig. 3. Volume-specific GFP production rates show the effect of positive and negative transcription regulation by DnaA-ATP and delayed induction after gene doubling by SeqA. (**A**) Plot of the conditional average of GFP volume-specific production rate from the *dnaA*P2 promoter as a function of cell volume. (**B**) The same average across mother + daughter lineages shows two minima at multiples of a characteristic volume, as expected from replication initiations. (**C**) Top: the m3SeqA promoter, reporting for DnaA activity, shows shifted oscillations with a shorter period and smaller amplitude with respect to *dnaA*P2. The plots are conditional averages of the volume-specific GFP production rate (plotted as fold change) as a function of volume (left) or cell-cycle phase (right). Vertical dashed lines show oscillation minima. The promoter repressed by DnaA-ATP presents oscillations within the cell cycle also when it is not regulated by SeqA (pink dashed lines) although the timing of the peaks is altered and the amplitude of the oscillation is smaller. A mean volume at the minima around 3.5 to 3.6 µm^3 roughly corresponds to the expected mean cell volume at the mean cell-cycle phase (shown in fig. S3C) corresponding to replication initiation in this condition. Bottom: Comparison of volume conditional averages for all promoters. The plots show the fold change of conditional averages of specific production rate with respect to cell volume for different promoters controlling the expression of GFP. The differences in amplitude and phase are consistent with SeqA delaying the increase in gene expression following gene duplication (comparison of no Act + noRepr with Constitutive), activation taking place after SeqA repression (compare Act + noRepr to noAct + noRepr) and DnaA-ATP repression taking place at a smaller volume than SeqA repression (compare Act + Repr to Act + noRepr).

We divided cells into 11 different birth size classes and considered binned averages of specific GFP production rate oscillations as a function of cell-cycle phase, time to division, time from birth, or cell volume. Figure 4A shows three of the birth size bins relative to an average birth size of 2.2 ± 0.1 μm^3, 2.4 ± 0.1 μm^3, and 2.6 ± 0.1 μm^3. The plots show that volume-binned oscillations are strongly insensitive to birth size, because the data for different birth size bins overlap, while the other variables are sensitive (i.e., the plots relative to different birth size classes do not collapse). Binning by time from birth shows that cells born larger reach the minimum of the oscillation in a shorter time than cells born smaller. Binning by time to division shows the same trend, but results in an intermediate level of collapse. To quantify this behavior, we defined a score of the collapse of different birth size classes as the inverse of the sum of SE-normalized distances between the oscillations in specific production rate for all 11 birth size bins (Fig. 4B). The higher the score, the greater the collapse of the oscillations for cells with a different birth size. Figure 4B shows that cell volume gives the highest score. Time to division gives an intermediate score (still a factor of 2 higher than those for cell-cycle phase and time from birth). Last, we compared the collapse score using different proxies of cell size (length, surface, and volume) as candidates to be sensed by the *dnaA*P2 oscillator, finding that volume is the best candidate (*50*) (fig. S5).

Volume-sensitive *dnaA*P2 oscillations require activation and repression by DnaA-ATP and are linked to cell division via repression by SeqA

As noted above, the binned averages of volume-specific GFP production as a function of cell volume for the constitutive promoter, the promoters stripped of DnaA-ATP binding sites and the m3SeqA promoter show oscillations that are lower than the ones seen for the wild-type *dnaA*P2 promoter, but still have an amplitude of 30 to 40% (Fig. 3C). Crucially, however, the analysis on the joint conditional averages as a function of birth volume reveals direct volume sensing more effectively (Fig. 5).

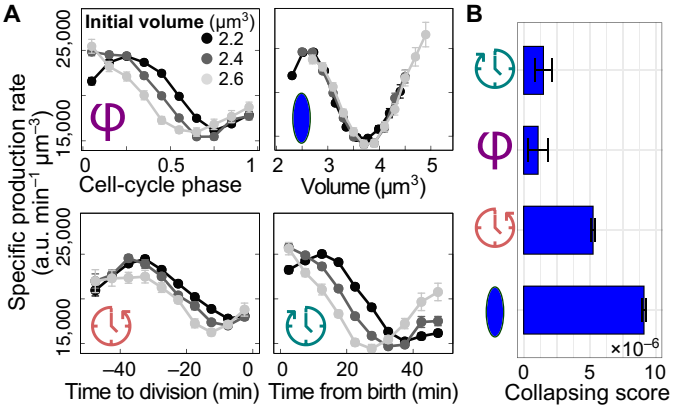

Fig. 4. *dnaA*P2 oscillations sense cell volume. (**A**) Volume-specific *dnaA*P2 promoter activity oscillations for cells of different initial size show different degrees of overlap when conditionally averaged as a function of cell-cycle phase, time to division, time from birth, and cell volume. The differently shaded curves result from data binned according to cell size (volume) at birth (2.2 ± 0.1 μm^3, black; 2.4 ± 0.1 μm^3, dark gray; and 2.6 ± 0.1 μm^3, light gray). If the variable in the *x* axis is the sensed variable, the averages should change independently of the cell size at birth. Data for cell volume show the best collapse, indicating that the *dnaA*P2 oscillator is a volume sensor. (**B**) Quantification of the collapse of the curves of (A) relative to 11 bins of cell sizes at birth (see Methods). Binning the data by cell size shows the best collapse and binning the data as a function of the time to division shows a good collapse. Error bars (often smaller than symbol size) are standard errors of the mean from a resampled distribution obtained by bootstrapping from the experimental data for each bin.

The comparison of the results of this volume-sensing analysis obtained with the different promoter constructs shows that the collapse score for volume is the highest for the wild-type *dnaA*P2 sequence, remains high for the mutants that are still activated by DnaA, and is lost when both DnaA binding sites are mutated (Fig. 5). Removing cell cycle–dependent repression by mutating the SeqA regulatory sites (m3SeqA reporter mutant) has a small effect on the collapse with volume but loses the collapse with the time to division (Fig. 5, and shown in detail in fig. S6). In other words, regulation by DnaA-ATP alone is not sufficient to link the oscillation in GFP production rate to the time of cell division, which seems to require repression by SeqA.

Last, regulation by SeqA alone (in the mutant promoter not regulated by DnaA) is insufficient to couple the oscillations to either volume or cell size at division independently of birth size (Fig. 5). Note that the population average gene expression level for this mutant is very similar to that of the wild type (fig. S1).

In summary, both positive and negative regulation by DnaA are required to maintain a good coordination between the oscillator and cell volume. An improved level of collapse of the curves is obtained by transcription repression from SeqA.

Together, these data lead us to conclude that the *dnaA*P2 oscillator sets its phase through the timing of SeqA regulation and the changes in gene copy number. These oscillations are amplified by volume-coupled DnaA-dependent transcription regulation due to the cycle of DnaA activity.

At the single-cell level, *dnaA*P2 oscillation minima are compatible with initiations

The analyses conducted thus far demonstrate the connection between the *dnaA*P2 oscillator, cell size, and cell division through conditional means. However, our data enable a more direct exploration of how the oscillations of single-cell *dnaA*P2 and m3SeqA relate to cell-cycle progression. Figures S7 and S8A show that, in our data, *dnaA*P2 oscillations are detectable in our single-cell tracks. We extracted for every cell and lineage the local minima of the *dnaA*P2 oscillations (Supplementary Notes).

We observed a bimodal distribution of cell sizes at minima, with their modes in a rough 1:2 ratio, as expected from initiations, which was lost in the m3seqA oscillator (fig. S8, B and C). Identifying *dnaA*P2 oscillation minima in single-cell lineages enabled us to perform the analysis reported in Fig. 4 (A and B) testing sensing of added volume (fig. S9), showing an equally good collapse, and to test for size-growth correlations between consecutive minima (figs. S10 and S11), as well as to compare these findings with those obtained with the m3SeqA promoter (Fig. 3C and fig. S11).

Overall, these results indicate that the *dnaA*P2 oscillator acts in synchrony with volume and with cell division similarly to replication initiations, while the m3SeqA oscillator, deprived of SeqA repression at fork passage and purely reporting on DnaA activity, loses some of these properties.

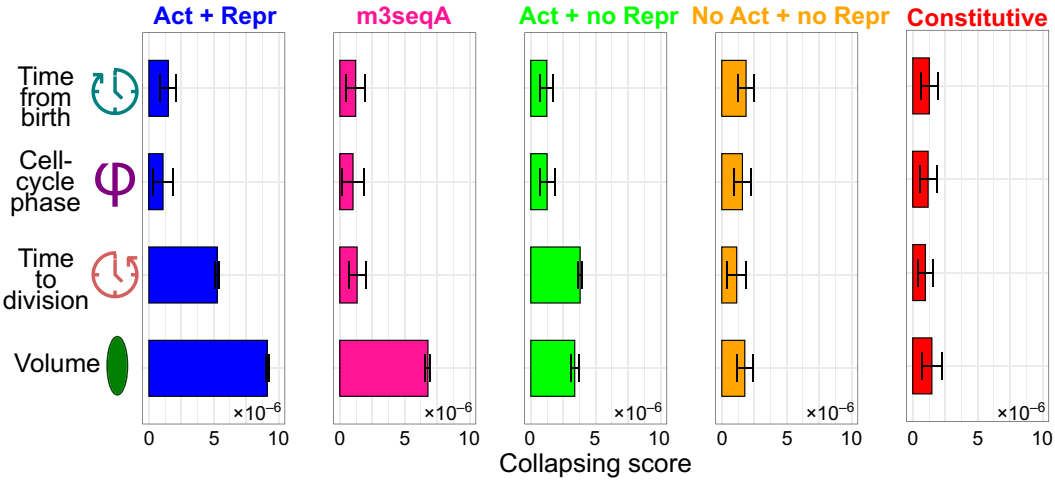

Fig. 5. DnaA regulation is essential for volume sensing. The plots test direct volume sensing across different mutant promoters, by quantifying the collapse score of conditional averages of specific production rate for classes with different initial sizes (see Fig. 4, A and B). The different panels compare collapse scores for volume sensing among different promoter constructs, and the first panel is identical to Fig. 4B. The wild-type *dnaA*P2 sequence shows the highest collapse score, is lowered for the reporter mutant still activated by DnaA, but is lost when both DnaA binding sites are mutated. The m3SeqA reporter mutant shows a minor impact on the volume collapse but eliminates the collapse with the time to division, suggesting that DnaA-ATP regulation alone is insufficient to connect the oscillation in volume-specific GFP production rate to the time of cell division, and that repression by SeqA is required. The collapse score defined in Fig. 4B is the SE-normalized inverse mean L_2 distance of conditional averages across bins of birth size.

Causal links with cell volume and division differ between *dnaA*P2 and m3seqA oscillations

Because the automated detection of the minima requires smoothing the data and taking derivatives, then smoothing again to detect minima reliably, this procedure is particularly sensitive to false positives due to propagated measurement noise. In addition, the analyses so far do not explicitly reveal the causal links between the DnaA oscillators and the cell division cycle.

To address possible causal links, we used synchronization analysis, cross-covariance, and causal inference of *dnaA*P2 time series along lineages of single cells. The two latter techniques in particular have the advantage of considering the whole time series (hence leveraging all the data) and not just relying on minima detection. For each lineage, we considered the *dnaA*P2 and m3SeqA cell-cycle oscillators, the cell volume time series, and the cell division time series, as three a priori independent signals, to investigate their synchronization and to test whether a causality between these signals exists (Fig. 6A and fig. S7). Each of these parameters displays some periodicity throughout several generations.

To test the presence of a time hierarchy connecting specific *dnaA*P2 activity and volume oscillations, we first considered the cross-covariance between these two time series, computed along lineages (*51*). Cross-covariance analysis measures the correlation between two time series at different time lags, helping to identify whether changes in one series tend to occur before or after changes in the other. We note that this analysis indicates the direction and delay of a potential causal influence between the variables, but does not support a causal relationship; it just indicates a sequential relationship. Figure 6B shows that the cross-covariance function exhibits a clear periodic pattern based on the delay time, which implies a tight connection between the two oscillating variables at a consistent phase difference. The function reveals higher positive peaks when volume changes occur before changes in *dnaA*P2 (positive time delays), rather than after (negative time delays), indicating that fluctuations in volume typically precede and possibly influence fluctuations in the *dnaA*P2 activity related to volume. In promoter mutants with mutated DnaA binding sites or in the constitutive promoter, the cross-covariances are strongly reduced (fig. S12). Mutation of SeqA binding sites (m3seqA) mildly reduces the amplitude of the delayed cross-covariances, and slightly alters the pattern of the time asymmetry (Fig. 6B and fig. S12).

Figure S13 (see Supplementary Notes) tests the phase locking between the *dnaA*P2 and m3SeqA oscillators with the cell cycle (*52*–*54*). While the *dnaA*P2 oscillator exhibits consistent phase differences, implying synchronization, the m3SeqA mutant disrupted this dependency, possibly indicating a loss of complete synchrony with the cell-cycle phase.

Because of the loss of synchronization with the cell cycle of the m3SeqA oscillator, and due to its loss of delay-time asymmetry in the cross-covariance with volume, we figured that the causal links between the oscillator and the other proxies of the cell cycle may be stronger for the wild-type *dnaA*P2 oscillator. While asymmetric cross-covariances reveal a time hierarchy, one has to be careful when inferring causal relations between two observables because the existence of a nonzero correlation between two signals does not necessarily imply a causal link (*52*). To investigate the directionality of the coupling, we used the convergent cross-mapping (CCM) technique, considering conditional correlations of one variable with a second one, under the constraint that the former is constrained to its attractor manifold, as reconstructed from the time series using Takens' theorem (*55*, *56*) (see Methods and fig. S14). CCM is a method able to detect causality between two time series by checking whether the historical states of one series can accurately predict the states of another. CCM operates under the premise that if one variable causally influences another, the dynamics of the first should be contained in the time series of the second, but not vice versa. In

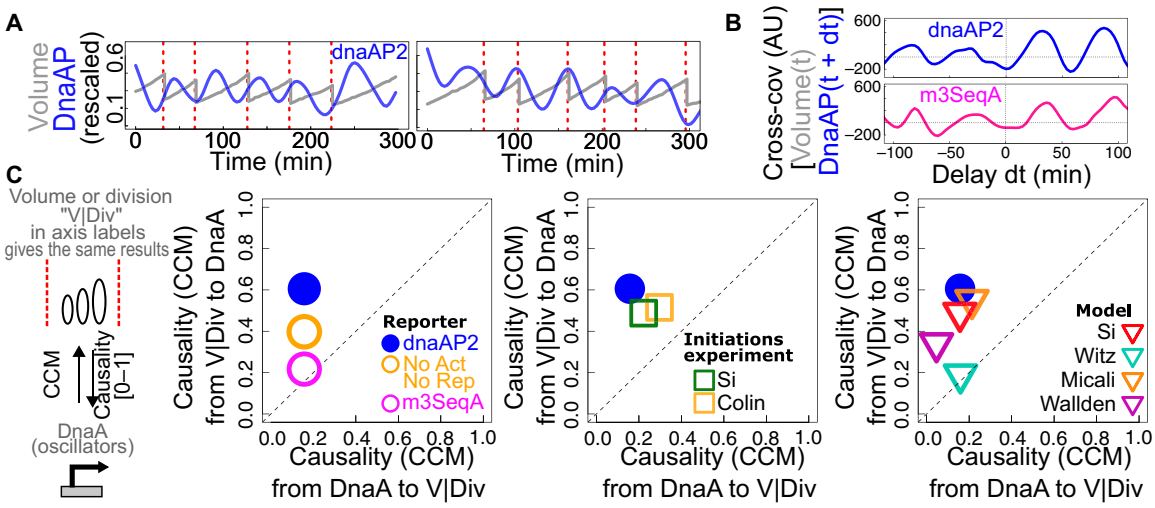

Fig. 6. *dnaA*P2 promoter activity and growth division are coupled oscillators. (**A**) Lineages of single cells show a clear oscillation of *dnaA*P2 promoter activity (blue), compared here to volume growth (gray) and division events (red), which we considered as three a priori independent time series. Volume and *dnaA*P2 promoter activity are normalized here by their average value to show them in the same plot. (**B**) Cross-covariance between *dnaA*P2 promoter activity and volume growth is periodic, supporting synchronization between the two oscillators, and asymmetric, supporting a stronger effect of volume changes on future *dnaA*P2 changes than vice versa. Asymmetry and cross-covariance are weaker for the m3SeqA oscillator. (**C**) CCM was used to detect causal relationships between oscillators. Cell volume and cell division give equivalent results in this analysis (fig. S15); hence, we report the results for both variables together (labels "V|Div" in the plots). Left: For the wild-type promoter, volume/division are strong causes of *dnaA*P2 changes, but the strength of this causal link decreases in the mutants of the DnaA binding sites, and the causality becomes completely symmetric in the mutant of the SeqA binding site. Middle: CCM derived from experimental replication-initiation datasets is consistent with our data for the wild-type promoter [the label "Si" corresponds to (*31*) and "Colin" corresponds to (*28*)]. Right: CCM from simulated initiation datasets is most consistent with our data for the wild-type *dnaA*P2 promoter for different models [the label "Si" corresponds to the model of (*31*) and "Micali" corresponds to the model used in (*28*–*30*); "Witz" corresponds to (*32*) and "Wallden" corresponds to (*34*)].

practice, this technique requires reconstructing the multidimensional phase space of each time series from the vectors of all observed delays, and looking for cases where knowing the trajectory of one variable helps to map out the trajectory of the other, which would reveal a causal link. This analysis is based on the whole time series and does not rely on minima detection. The output of this analysis, given two time series A and B is a pair of a directional parameters ρ_{AB} and ρ_{BA}, between 0 and 1, that represent the strength of the causality link from A to B and from B to A, respectively. A causal relationship is witnessed by unequal causality parameters in the two directions $\rho_{AB} \neq \rho_{BA}$. For example, if A causes B, we expect that $\rho_{AB} > \rho_{BA}$.

Figure 6C summarizes the results of this analysis on our data. To try to disentangle the effects of cell volume from cell division events, we first tested the causality between cell volume and an oscillatory signal constructed to have a maximum at division. This analysis returns that volume and cell division are always in a strong symmetric relationship (fig. S15); hence, they are causally indistinguishable. Crucially, Fig. 6C shows instead a strongly asymmetric causality from volume (or division) to *dnaA*P2. This asymmetric causal link is weakened in the promoter without negative and positive DnaA regulation, and disappears in the m3SeqA promoter, for which the correlation becomes causally symmetric. It is important to point out that these results do not refer to the mutant of the endogenous *dnaA* promoter, but only report how the same endogenous DnaA-ATP oscillations and SeqA transit are read by our reporters when there are mutations of the binding sites. Hence, the observation that causality is lost when SeqA binding sites (and thus sensing of the passage of the replication fork) are mutated indicates once again that the endogenous *dnaA* promoter and our reporter take relevant input from the fork transit.

Because we have found that *dnaA*P2 oscillatory minima in single cells follow similar patterns to those found for initiation events, we devised a way to compare the oscillator's causality patterns with those observed for initiations, both in data from (*28*, *31*) and in cell-cycle mathematical models proposed in the literature (*28*–*32*, *34*) (Fig. 6C). To do this, we constructed time series connecting measured or simulated initiation events by sinusoids, in such a way that the minima coincide with initiations in time series taken from data or mathematical models (see Methods). This procedure produces a differentiable oscillatory curve, which can be compared to volume and division time series using CCM. Figure 6C shows that the predicted causality pattern from experimental data on initiations is completely consistent with the one shown by *dnaA*P2. Figure 6C shows that only the models from (*29*, *31*) are consistent with the causal asymmetry. Both models assume that the pattern between initiations is an adder per origin. The model proposed by Si and coworkers assumes that division is agnostic of the chromosome, and not linked to replication-segregation. The concurrent processes model proposed by Micali and coworkers assumes concurrency of timescales between a cellular process and chromosome replication-segregation setting division through an AND gate.

Going back to our experimental data from wild-type *dnaA*P2, our causality analysis using CCM shows that cell division or cell size cause *dnaA*P2 oscillations in a much stronger fashion than *dnaA*P2 causes division. This perhaps unintuitive result may have two explanations: (i) there is a strong symmetric coupling between cell division and cell size, and the *dnaA*P2 promoter is a strong size sensor,

or (ii) there is a strong symmetric coupling between cell division and cell size, and the *dnaA*P2 promoter is a strong cell division sensor. However, the causal equivalence of cell division and volume in our data does not allow us to distinguish between the two hypotheses. Note that given the essentiality of the SeqA binding sites for the causal asymmetry, it seems reasonable to assume that the crucial sensed event is fork transit; hence, the above hypotheses could be restated by saying (i) that replication initiation itself may be a strong sensor of the previous cell division and (ii) that it may be a strong sensor of cell size.

To attempt to resolve this question, we performed additional experiments inhibiting division by adding cephalexin (fig. S16). Cephalexin-treated cells do not divide, but continue to grow and initiate DNA replication, producing an array of nucleoids. Hence, their cell cycle is still somewhat operative. CCM analysis is technically impossible under this perturbation, because the volume time series increases monotonically and lacks an attractor. This perturbation does not ablate time-periodic *dnaA*P2 oscillations (fig. S16), but conditional averages become flat as soon as the cell sizes exceed the physiological range, suggesting that the synchrony with cell volume is lost (*57*).

DISCUSSION

In summary, here we have measured oscillations in DnaA activity and SeqA repression that integrate the effects from several regulatory mechanisms to regulate the initiation of DNA replication. Given the essential role of DnaA in cell growth and adaptation, these processes regulate its activity to maintain a stable DNA replication program across growth conditions (*58*–*60*).

Our results show that oscillations in volume-specific gene expression rate are also observed for an unregulated promoter, likely as a result of the changes of gene, mRNA, and ribosome copy number with cell volume. However, we also show that the pattern of gene expression from the *dnaA* promoter differs substantially from this pattern. By the comparison of different promoter variants and cell size dynamics, we show that the expression of the wild-type *dnaA* gene is tightly coupled to volume and senses a successful initiation via SeqA repression.

Specifically, we know that volume coupling of the oscillator needs DnaA-ATP regulation of the promoter as we see that in the presence of this regulatory element, the oscillator is strongly coupled to volume, and this property is lost in the mutants. Our results rigorously demonstrate that the rate of *dnaA*P2 expression is tightly coupled to cell volume ("size"). Moreover, this correlation results from a causative relationship in which volume determines expression. Equally importantly, *dnaA*P2 oscillations are insensitive to cell size at birth, thus excluding one otherwise possible regulation point. The volume correlation is tighter than that seen from two potentially volume-correlated effects, cell length and cell surface area. These results thus provide strong evidence that cell volume is crucial for the production of DnaA-ATP and, thus, by extension, the occurrence of replication initiation. This volume-coupled cell-cycle oscillator should be taken into account while modeling *E. coli* cycle control.

Our cephalexin results could also suggest that sustained DnaA activity oscillations do not rely on periodic volume reset by cell division to be in place but depend on a variable that is strongly synchronized to volume in dividing cells. Cell division could be partly responsible for this synchronization. Presumably, origin density oscillations are rather conserved in cephalexin-treated nondividing cells, hence the results may also argue against the DnaA-P2 oscillator being strongly coupled to origin density. However, these considerations remain speculative and need to be tested in future studies.

Despite the clear results on the coupling between cell volume and DnaA activity oscillations, our current data do not allow us to determine directly whether, at the single-cell level, they are also coupled to the initiation of DNA replication, apart from the effect of SeqA on the wild-type promoter. Future work will investigate whether the stochasticity in gene expression is reflected in the initiation process. This approach will help identify the other processes contributing to the robustness of initiation.

While linkage of *dnaA*P2 expression to volume is mediated by DnaA-ATP to its P2 binding sites, irrespective of SeqA, our results also show that in the absence of SeqA, the synchronization of the *dnaA*P2 oscillator with cycle progression becomes weaker, and P2 binding of SeqA alters the relationship between volume and expression, shifting the phase of the relationship to higher volumes. This effect is expected given that SeqA repression transiently prolongs the low expression state that immediately follows replication initiation. As a result, a volume-dependent increase, and thus initiation, will occur at larger volumes. The functional significance of this feature is that it provides a longer period of low DnaA-ATP concentration following initiation, which, in turn, will sharpen the eventual response of initiation to increased DnaA-ATP concentration.

These findings provide a picture of the critical events that determine the timing of replication initiation. A possible interpretation is the following: DnaA-ATP peaks may be a necessary but not sufficient condition for initiation, or there may be an inherent stochasticity between reaching an activity peak and completing a successful initiation (in line with the observed weak correlation of the *dnaA*P2 oscillator to the time of division). Hence, there is a waiting time between an oscillation peak and an initiation, which varies from cycle to cycle. This waiting time tends to put the *dnaA*P2 oscillator off phase with the cell cycle. However, repression from SeqA may act as a sensor of the occurrence and timing of a successful initiation, which acts on the DnaA-P2 production rate in a way that puts it back in synchrony with cell-cycle progression (*13*).

Our results argue against several proposed cell-cycle models, and hence, they are a useful contribution to that debate. They are consistent with two quantitative models for cell-cycle control, one of which places all regulation at the time of division (*31*), and the other proposes inputs from both the chromosomal and cell division programs (*29*, *30*). While our results do not directly allow us to distinguish between the two models, the weak correlation of *dnaA*P2 expression with cell division could potentially favor the second model.

Our findings are in line with recent RNA quantification data in fixed cells as a function of DNA content and cell size measurements (*61*), but the dynamic resolution of our data allows for a causal coupling analysis that indicates a directional causality between the oscillator and cell-cycle progression, contingent upon SeqA repression. Because absence of SeqA repression also weakens the causal relationship, our results suggest that while DnaA-ATP peaks play a key role in replication initiation, DnaA activity might not be the sole trigger. Rather, it may serve as a necessary but not sufficient condition or necessitates assistance from another closely associated process (*62*). This result on the causality is also reflected in a weakening

of the synchronization of the oscillator with cell division for m3seqA, and on the fact that the correlation pattern of oscillatory minima does not tightly follow the initiation pattern, although these two analyses rely on possibly noisy minima detection.

Coherently with this interpretation, recent systematic analyses of mutants (*63*, *64*) indicate that functional initiation of DNA replication can still take place in the absence of most regulatory factors, provided sufficient amounts of DnaA-ATP are available. Last, transient transcription repression by SeqA and titration of DnaA on genomic sites were proposed to lead to steeper oscillations in DnaA activity (*11*, *13*, *65*). We propose that the shutoff of gene expression following initiation may also play a role by resetting the DnaA-ATP dependent oscillation in DnaA expression, thus linking subsequent initiation events to a DnaA activity–based cell volume sensor.

METHODS

Strains and growth media

The experiments were carried out with the wild-type *E. coli* strain BW25113, the parent strain of the Keio collection (*66*), which has been fully sequenced (*67*). Promoter-reporter constructs were inserted in the chromosome close to the origin of replication at Ori3 (4,413,507 bp, in the region downstream of the converging *aidB* and *yjfN* genes). The *gfpmut2* gene, coding for a fast-folding GFP (*38*), is placed downstream of the chosen promoter sequence. A kanamycin resistance cassette (KanR) is divergently expressed upstream from the promoter region. The constitutive promoter cassette was also inserted in the chromosome close to the replication terminus, at the Ter3 site (1,395,706 bp, downstream of the converging *uspE* and *ynaJ* genes). Bacteria were grown overnight in M9 + 0.4% glucose at 30°C. Overnight cultures were diluted 500:1 in new growth medium and returned to the incubator for 3 to 4 hours. This is important to guarantee bacteria to be in the exponential phase when injected into the microfluidic device. Experiments were carried out at 30°C in M9 + 0.4% glucose + 0.2% casamino acids, with an average doubling time of 45 ± 5 min. We verified that the different levels of expression of the GFP in the different strains do not have an effect on cell growth. Doubling time and cell size are consistent between all the mutants (fig. S17).

Mother machine experiments

We used a microfluidic "mother machine" device where the 1-μm channels are found between two large feeding channels (*68*). The bacteria are trapped in the microfluidic channel thanks to a narrower opening on one side. PDMS (polydimethylsiloxane) devices from the mold were obtained by standard procedure and attached to a microscope slide by treatment with a plasma cleaner. Before loading bacteria into the device, each chip was treated with a solution of bovine serum albumin (BSA) to minimize bacterial interactions and binding to the glass or PDMS components. Devices were injected with around 150 μl of 2% BSA and incubated at 30°C for 1 hour. Passivated chips were rinsed with freshly filtered medium and 1 ml of bacterial culture was injected manually. Each feeding channel is coupled with a flow sensor. Using its feedback loop, we can monitor and control the flow rate in our microfluidic setup while keeping the stability and responsiveness of air pressure-driven flows (Elveflow). This technology enables us to set up robust and long-term microfluidic experiments. A home-built temperature control system is used to maintain the entire setup at 30°C. We use Nikon Inverted Microscope ECLIPSE Ti-E with a 100× oil objective, high–numerical aperture (1.4) lens, coupled with a Nikon Perfect Focus System to rectify drift in focus. An xy motion plate is used to memorize and loop over different regions of interest at a specified time interval.

The camera captured 16 bit images at 512 × 512 pixel resolution with the length of 1 pixel equal to 0.1067 μm. The motorized stage and camera were programmed to cycle between at most 40 fields of view, each spanning roughly eight microchannels, every 3 min.

Data analysis pipeline

The data obtained are in the .nd2 format and are imported and analyzed with the Fiji-ImageJ software. Background subtraction is performed using a 50-pixel rolling ball technique, and different positions are stored separately as a set of .tiff image files. Channels with a good number of bacteria are selected manually and stored in different folders. For segmentation and tracking, we started from codes developed by Panlilio *et al.* (*40*), and we added necessary modifications to optimize them for our experimental setup. Before starting, we select the experimental time window where bacteria were growing in a steady growth rate in a given growth medium. This window was defined by observing sliding averages of population interdivision time, growth rate, and cell size at birth (*40*). To correct for segmentation and tracking errors, we applied a set of filters. First, we considered only cells where both mother and daughter(s) were at least partially tracked. Second, we excluded division events where daughters had a volume outside of the interval 40 to 60% of the volume of the mother. This step aims to eliminate filamentous cells and segmentation artifacts. Third, we excluded cell cycles with interdivision times lower than 15 min (the physiological lower limit is 15 to 20 min). Last, we considered cell cycles where initial/final volume, initial/final width, and initial/final growth rate were inside the 95% tails of the distribution. Before computing the discrete derivative of fluorescence and volume (as central derivatives defined across three subsequent frames), we removed outliers (defined by subtracting a trend line by binned averages and identifying points lying more than 1.5 SDs from the baseline) from fluorescence and volume traces and we substituted them by linear interpolation. Minima were detected after removing outliers from the differentiated data and smoothing with a three-point average.

All datasets were grouped based on strain in different R objects. We performed an exploratory data analysis to check whether datasets were consistent and whether filters worked as desired. Custom functions were written to handle and analyze these large, nonuniform datasets. In particular, functions were written to compute the discrete derivatives and the different normalizations.

Volume and gene dosage estimation

We calculate the volume describing a cell as a cylinder with two hemispherical caps

$$V(t) = \pi\left[\mathrm{l(t)} - \mathrm{w}\right]\left(\frac{w}{2}\right)^2 + \frac{4}{3}\pi\left(\frac{w}{2}\right)^3 \quad (1)$$

where w was taken as a cell-cycle average of the average measured cell width. The expected gene copy number was computed from the Cooper-Helmstetter model (*49*). Replication of the *E. coli* chromosome begins from a single origin, and oppositely oriented replication forks proceed symmetrically along the genome to complete replication. Since, on average, a cell divides at a time $C + D$ (≈60 min)

after replication initiation, an average time lag B before initiation is necessary to make the total replication time $B + C + D$ an integer multiple of the doubling time τ. Thus, defining $n = \mathrm{Int}[(C + \mathrm{D})/\tau]$ as the integer number of times that τ divides $C + D$, one has that $B + C + D = (n + 1)\tau$. More generally, we can consider a gene at a chromosomal position defined by its normalized distance from Ori; i.e., $l = 0$ represents a gene in Ori and $l = 1$ represents a gene in Ter. The copy number of this gene, g, changes during the cell cycle following

$$g(t) := \begin{cases} 2n' & \text{if } 0 < t < (n'+1)\tau - \left[c(1-l)+D\right] \\ 2n'+1 & \text{if } (n'+1)\tau - \left[c(1-l)+D\right] < t < \tau \end{cases} \quad (2)$$

where $n' = \mathrm{Int}\left[\frac{C(1-l)+D}{\tau}\right]$. By averaging over the cell cycle, one gets the expected average gene copy number

$$g = \langle g(t) \rangle_{\text{cell cycle}} = \frac{1}{\tau}\int_0^\tau g(t)dt = 2^n\left\{1 - n + \mu\left[C(1-l)+D\right]\right\} \quad (3)$$

Convergent cross-mapping

CCM is a method for causality inference based on Takens' theorem (*55*) and developed in (*56*). Takens' theorem shows that time-delay embedding of a one-dimensional time series provides a 1-1 mapping of system dynamics from the original phase space (constructed with all system variables) to the reconstructed shadow phase space, as long as the latter has sufficient dimensions to contain the original attractor. Figure S14 summarizes the main steps of the CCM method. Shortly, it reconstructs a shadow attractor from one time series at a time and uses these coordinates to compute conditional correlations at fixed values of the shadow attractor of the variable. Because they are based on different constraints, the conditional correlations are not symmetric and reveal causal links. We used the R package multispatialCCM to implement CCM (https://CRAN.R-project.org/package=multispatialCCM) (*69*). CCM was used on our experimental data on volume, divisions, and *dnaA*P2 oscillation time series, using DNA replication initiation data from the literature and on simulated data. In our data, we used volume and *dnaA*P2 oscillator time series, and a cell division time series was defined as a continuous process with narrow peaks around each experimental division event. For initiation of DNA replication data, we used two datasets from the literature where initiation of DNA replication and cell division were tracked within the cell cycle (*28*, *31*), and we defined a putative *dnaA*P2 oscillator time series by assuming a sinusoid between 0 and 1 with the minima at consecutive initiations (fig. S14B). We also simulated four different models described in the literature: a model where replication initiation sets cell division through a timer, from (*34*); a model where DNA replication initiation sets cell division through an adder (*32*); a model where replication and an inter-division concurrently limit cell division (*29*, *30*); and a model where DNA replication has no direct influence on the timing of division (*31*). The codes and parameter values are those used in (*28*).

Supplementary Materials

This PDF file includes:

Table S1
Supplementary Notes
Figs. S1 to S17
References

REFERENCES AND NOTES

1. R. Ohbayashi, S. Hirooka, R. Onuma, Y. Kanesaki, Y. Hirose, Y. Kobayashi, T. Fujiwara, C. Furusawa, S. Y. Miyagishima, Evolutionary changes in DnaA-dependent chromosomal replication in cyanobacteria. *Front. Microbiol.* **11**, 786 (2020).
2. A. C. Leonard, P. Rao, R. P. Kadam, J. E. Grimwade, Changing perspectives on the role of DnaA-ATP in orisome function and timing regulation. *Front. Microbiol.* **10**, 2009 (2019).
3. K. E. Duderstadt, M. L. Mott, N. J. Crisona, K. Chuang, H. Yang, J. M. Berger, Origin remodeling and opening in bacteria rely on distinct assembly states of the DnaA initiator. *J. Biol. Chem.* **285**, 28229–28239 (2010).
4. J. P. Erzberger, M. L. Mott, J. M. Berger, Structural basis for ATP-dependent DnaA assembly and replication-origin remodeling. *Nat. Struct. Mol. Biol.* **13**, 676–683 (2006).
5. D. Bramhill, A. Kornberg, Duplex opening by dnaA protein at novel sequences in initiation of replication at the origin of the *E. coli* chromosome. *Cell* **52**, 743–755 (1988).
6. A. Lobner-Olesen, K. Skarstad, F. G. Hansen, K. von Meyenburg, E. Boye, The DnaA protein determines the initiation mass of *Escherichia coli* K-12. *Cell* **57**, 881–889 (1989).
7. N. S. Hill, R. Kadoya, D. K. Chattoraj, P. A. Levin, Cell size and the initiation of DNA replication in bacteria. *PLOS Genet.* **8**, e1002549 (2012).
8. F. Si, D. Li, S. E. Cox, J. T. Sauls, O. Azizi, C. Sou, A. B. Schwartz, M. J. Erickstad, Y. Jun, X. Li, S. Jun, Invariance of initiation mass and predictability of cell size in *Escherichia coli*. *Curr. Biol.* **27**, 1278–1287 (2017).
9. H. Zheng, Y. Bai, M. Jiang, T. A. Tokuyasu, X. Huang, F. Zhong, Y. Wu, X. Fu, N. Kleckner, T. Hwa, C. Liu, General quantitative relations linking cell growth and the cell cycle in *Escherichia coli*. *Nat. Microbiol.* **5**, 995–1001 (2020).
10. T. Katayama, K. Kasho, H. Kawakami, The DnaA cycle in *Escherichia coli*: Activation, function and inactivation of the initiator protein. *Front. Microbiol.* **8**, 2496 (2017).
11. F. G. Hansen, T. Atlung, The DnaA tale. *Front. Microbiol.* **9**, 319 (2018).
12. E. Boye, A. Lobner-Olesen, K. Skarstad, Limiting DNA replication to once and only once. *EMBO Rep.* **1**, 479–483 (2000).
13. J. L. Campbell, N. Kleckner, *E. coli* oriC and the dnaA gene promoter are sequestered from dam methyltransferase following the passage of the chromosomal replication fork. *Cell* **62**, 967–979 (1990).
14. L. Riber, A. Lobner-Olesen, Coordinated replication and sequestration of oriC and dnaA are required for maintaining controlled once-per-cell-cycle initiation in *Escherichia coli*. *J. Bacteriol.* **187**, 5605–5613 (2005).
15. M. Lu, J. L. Campbell, E. Boye, N. Kleckner, SeqA: A negative modulator of replication initiation in *E. coli*. *Cell* **77**, 413–426 (1994).
16. P. W. Theisen, J. E. Grimwade, A. C. Leonard, J. A. Bogan, C. E. Helmstetter, Correlation of gene transcription with the time of initiation of chromosome replication in *Escherichia coli*. *Mol. Microbiol.* **10**, 575–584 (1993).
17. M. A. Sánchez-Romero, S. J. W. Busby, N. P. Dyer, S. Ott, A. D. Millard, D. C. Grainger, Dynamic distribution of SeqA protein across the chromosome of *Escherichia coli* K-12. *mBio* **1**, e00012 (2010).
18. T. Atlung, E. S. Clausen, F. G. Hansen, Autoregulation of the dnaA gene of *Escherichia coli* K12. *Mol. Gen. Genet.* **200**, 442–450 (1985).
19. C. Speck, C. Weigel, W. Messer, ATP- and ADP-DnaA protein, a molecular switch in gene regulation. *EMBO J.* **18**, 6169–6176 (1999).
20. C. Saggioro, A. Olliver, B. Sclavi, Temperature-dependence of the DnaA–DNA interaction and its effect on the autoregulation of dnaA expression. *Biochem. J.* **449**, 333–341 (2013).
21. R. E. Braun, K. O'Day, A. Wright, Autoregulation of the DNA replication gene dnaA in *E. coli* K-12. *Cell* **40**, 159–169 (1985).
22. J.-i. Kato, T. Katayama, Hda, a novel DnaA-related protein, regulates the replication cycle in *Escherichia coli*. *EMBO J.* **20**, 4253–4262 (2001).
23. K. Kasho, T. Katayama, DnaA binding locus datA promotes DnaA-ATP hydrolysis to enable cell cycle-coordinated replication initiation. *Proc. Natl. Acad. Sci. U.S.A.* **110**, 936–941 (2013).
24. K. Fujimitsu, T. Senriuchi, T. Katayama, Specific genomic sequences of *E. coli* promote replicational initiation by directly reactivating ADP-DnaA. *Genes Dev.* **23**, 1221–1233 (2009).
25. J. Frimodt-Mller, G. Charbon, K. A. Krogfelt, A. Lobner-Olesen, DNA replication control is linked to genomic positioning of control regions in *Escherichia coli*. *PLOS Genet.* **12**, e1006286 (2016).
26. K. Miyoshi, Y. Tatsumoto, S. Ozaki, T. Katayama, Negative feedback for DARS2-Fis complex by ATP-DnaA supports the cell cycle-coordinated regulation for chromosome replication. *Nucleic Acids Res.* **49**, 12820–12835 (2021).
27. W. D. Donachie, G. W. Blakely, Coupling the initiation of chromosome replication to cell size in *Escherichia coli*. *Curr. Opin. Microbiol.* **6**, 146–150 (2003).
28. A. Colin, G. Micali, L. Faure, M. Lagomarsino, S. van Teeffelen, Two different cell-cycle processes determine the timing of cell division in *Escherichia coli*. *eLife* **10**, e67495 (2021).
29. G. Micali, J. Grilli, M. Osella, M. C. Lagomarsino, Concurrent processes set *E. coli* cell division. *Sci. Adv.* **4**, eaau3324 (2018).

30. G. Micali, J. Grilli, J. Marchi, M. Osella, M. Cosentino Lagomarsino, Dissecting the control mechanisms for DNA replication and cell division in *E. coli*. *Cell Rep.* **25**, 761–771.e4 (2018).
31. F. Si, G. le Treut, J. T. Sauls, S. Vadia, P. A. Levin, S. Jun, Mechanistic origin of cell-size control and homeostasis in bacteria. *Curr. Biol.* **29**, 1760–1770.e7 (2019).
32. G. Witz, E. van Nimwegen, T. Julou, Initiation of chromosome replication controls both division and replication cycles in *E. coli* through a double-adder mechanism. *eLife* **8**, e48063 (2019).
33. A. Adiciptaningrum, M. Osella, M. C. Moolman, M. Cosentino Lagomarsino, S. J. Tans, Stochasticity and homeostasis in the *E. coli* replication and division cycle. *Sci. Rep.* **5**, 18261 (2016).
34. M. Wallden, D. Fange, E. G. Lundius, O. Baltekin, J. Elf, The synchronization of replication and division cycles in individual *E. coli* cells. *Cell* **166**, 729–739 (2016).
35. S. Tiruvadi-Krishnan, J. Männik, P. Kar, J. Lin, A. Amir, J. Männik, Coupling between DNA replication, segregation, and the onset of constriction in *Escherichia coli*. *Cell Rep.* **38**, 110539 (2022).
36. W. Messer, C. Weigel, DnaA as a transcription regulator. *Methods Enzymol.* **370**, 338–349 (2003).
37. I. P. Menikpurage, K. Woo, P. E. Mera, Transcriptional activity of the bacterial replication initiator DnaA. *Front. Microbiol.* **12**, 662317 (2021).
38. B. P. Cormack, R. H. Valdivia, S. Falkow, FACS-optimized mutants of the green fluorescent protein (GFP). *Gene* **173**, 33–38 (1996).
39. O. Espeli, R. Mercier, F. Boccard, DNA dynamics vary according to macrodomain topography in the *E. coli* chromosome. *Mol. Microbiol.* **68**, 1418–1427 (2008).
40. M. Panlilio, J. Grilli, G. Tallarico, I. Iuliani, B. Sclavi, P. Cicuta, M. C. Lagomarsino, Threshold accumulation of a constitutive protein explains *E. coli* cell-division behavior in nutrient upshifts. *Proc. Natl. Acad. Sci. U.S.A.* **118**, e2016391118 (2021).
41. E. B. Hansen, F. G. Hansen, K. von Meyenburg, The nucleotide sequence of the dnaA gene and the first part of the dnaN gene of *Escherichia coli* K-12. *Nucleic Acids Res.* **10**, 7373–7385 (1982).
42. A. Travers, G. Muskhelishvili, DNA supercoiling—A global transcriptional regulator for enterobacterial growth? *Nat. Rev. Microbiol.* **3**, 157–169 (2005).
43. A. E. Chiaramello, J. W. Zyskind, Expression of *Escherichia coli* dnaA and mioC genes as a function of growth rate. *J. Bacteriol.* **171**, 4272–4280 (1989).
44. W. Messer, C. Weigel, DnaA initiator—Also a transcription factor. *Mol. Microbiol.* **24**, 1–6 (1997).
45. T. G. Wilkinson II, G. C. Kedar, C. Lee, E. C. Guzmán, D. W. Smith, J. W. Zyskind, The synchrony phenotype persists after elimination of multiple GATC sites from the dnaA promoter of *Escherichia coli*. *J. Bacteriol.* **188**, 4573–4576 (2006).
46. G. C. Kedar, F. Ozcan, E. C. Guzmán, D. W. Smith, V. G. Newman, J. W. Zyskind, Role of DNA methylation at GATC sites in the dnaA promoter, dnaAp2. *J. Mol. Microbiol. Biotechnol.* **2**, 301–310 (2000).
47. Z. Long, A. Olliver, E. Brambilla, B. Sclavi, M. C. Lagomarsino, K. D. Dorfman, Measuring bacterial adaptation dynamics at the single-cell level using a microfluidic chemostat and time-lapse fluorescence microscopy. *Analyst* **139**, 5254–5262 (2014).
48. N. Walker, P. Nghe, S. J. Tans, Generation and filtering of gene expression noise by the bacterial cell cycle. *BMC Biol.* **14**, 11 (2016).
49. S. Cooper, C. E. Helmstetter, Chromosome replication and the division cycle of *Escherichia coli*. *J. Mol. Biol.* **31**, 519–540 (1968).
50. H. Zheng, P.-Y. Ho, M. Jiang, B. Tang, W. Liu, D. Li, X. Yu, N. E. Kleckner, A. Amir, C. Liu, Interrogating the *Escherichia coli* cell cycle by cell dimension perturbations. *Proc. Natl. Acad. Sci. U.S.A.* **113**, 15000–15005 (2016).
51. D. J. Kiviet, P. Nghe, N. Walker, S. Boulineau, V. Sunderlikova, S. J. Tans, Stochasticity of metabolism and growth at the single-cell level. *Nature* **514**, 376–379 (2014).
52. A. Pikovsky, M. Rosenblum, J. Kurths, *Synchronization: A Universal Concept in Nonlinear Sciences* (Cambridge Univ. Press, 2003).
53. R. E. Goldstein, M. Polin, I. Tuval, Noise and synchronization in pairs of beating eukaryotic flagella. *Phys. Rev. Lett.* **103**, 168103 (2009).
54. J. Kotar, M. Leoni, B. Bassetti, M. C. Lagomarsino, P. Cicuta, Hydrodynamic synchronization of colloidal oscillators. *Proc. Natl. Acad. Sci. U.S.A.* **107**, 7669–7673 (2010).
55. F. Takens, Dynamical systems and turbulence, Warwick 1980, in *Lecture Notes in Mathematics*, D. Rand, L.-S. Young, Eds. (Springer, 1981), pp. 366–381.
56. G. Sugihara, R. May, H. Ye, C. H. Hsieh, E. Deyle, M. Fogarty, S. Munch, Detecting causality in complex ecosystems. *Science* **338**, 496–500 (2012).
57. A. Sánchez-Gorostiaga, P. Palacios, R. Martínez-Arteaga, M. Sánchez, M. Casanova, M. Vicente, B. Michel, W. Vollmer, D. Daley, Life without division: Physiology of *Escherichia coli* FtsZ-deprived filaments. *mBio* **7**, e01620 (2016).
58. V. A. Sutera, S. T. Lovett, The role of replication initiation control in promoting survival of replication fork damage. *Mol. Microbiol.* **60**, 229–239 (2006).
59. L. Riber, J. Frimodt-Mller, G. Charbon, A. Lobner-Olesen, Multiple DNA binding proteins contribute to timing of chromosome replication in *E. coli*. *Front. Mol. Biosci.* **3**, 29 (2016).
60. K. Kasho, S. Ozaki, T. Katayama, IHF and Fis as *Escherichia coli* cell cycle regulators: Activation of the replication origin oriC and the regulatory cycle of the DnaA initiator. *Int. J. Mol. Sci.* **24**, 11572 (2023).
61. A. W. Pountain, P. Jiang, T. Yao, E. Homaee, Y. Guan, M. Podkowik, B. Shopsin, V. J. Torres, I. Golding, I. Yanai, Transcription-replication interactions reveal principles of bacterial genome regulation. *Nature* **626**, 661–669 (2024).
62. E. Boye, T. Stokke, N. Kleckner, K. Skarstad, Coordinating DNA replication initiation with cell growth: Differential roles for DnaA and SeqA proteins. *Proc. Natl. Acad. Sci. U.S.A.* **93**, 12206 (1996).
63. A. Knöppel, O. Broström, K. Gras, D. Fange, J. Elf, Regulatory elements coordinating initiation of chromosome replication to the *Escherichia coli* cell cycle. *Proc. Natl. Acad. Sci. U.S.A.* **120**, e2213795120 (2023).
64. T. Boesen, G. Charbon, H. Fu, C. Jensen, D. Li, S. Jun, A. Lobner-Olesen, Robust control of replication initiation in the absence of DnaA-ATP ⇋ DnaA-ADP regulatory elements in *Escherichia coli*.
65. M. Berger, P. R. T. Wolde, Robust replication initiation from coupled homeostatic mechanisms. *Nat. Commun.* **13**, 6556 (2022).
66. T. Baba, T. Ara, M. Hasegawa, Y. Takai, Y. Okumura, M. Baba, K. A. Datsenko, M. Tomita, B. L. Wanner, H. Mori, Construction of *Escherichia coli* K-12 in-frame, single-gene knockout mutants: The Keio collection. *Mol. Syst. Biol.* **2**, 2006.0008 (2006).
67. F. Grenier, D. Matteau, V. Baby, S. Rodrigue, Complete genome sequence of *Escherichia coli* BW25113. *Genome Announc.* **2**, e01038-14 (2014).
68. Z. Long, E. Nugent, A. Javer, P. Cicuta, B. Sclavi, M. Cosentino Lagomarsino, K. D. Dorfman, Microfluidic chemostat for measuring single cell dynamics in bacteria. *Lab. Chip.* **13**, 947–954 (2013).
69. T. Clark, H. Ye, F. Isbell, E. R. Deyle, J. Cowles, G. D. Tilman, G. Sugihara, Spatial convergent cross mapping to detect causal relationships from short time series. *Ecology* **96**, 1174–1181 (2015).
70. N. Brenner, C. M. Newman, D. Osmanović, Y. Rabin, H. Salman, D. L. Stein, Universal protein distributions in a model of cell growth and division. *Phys. Rev. E Stat. Nonlin. Soft Matter Phys.* **92**, 042713 (2016).
71. L. Fernandez-Coll, M. Maciag-Dorszynska, K. Tailor, S. Vadia, P. A. Levin, A. Szalewska-Palasz, M. Cashel, The absence of (p)ppGpp renders initiation of *Escherichia coli* chromosomal DNA synthesis independent of growth rates. *mBio* **11**, e03223 (2020).
72. M. Osella, S. J. Tans, M. Cosentino Lagomarsino, Step by step, cell by cell: Quantification of the bacterial cell cycle. *Trends Microbiol.* **25**, 250–256 (2017).
73. P.-Y. Ho, A. Amir, Simultaneous regulation of cell size and chromosome replication in bacteria. *Front. Microbiol.* **6**, 662 (2015).
74. M. Campos, I. V. Surovtsev, S. Kato, A. Paintdakhi, B. Beltran, S. E. Ebmeier, C. Jacobs-Wagner, A constant size extension drives bacterial cell size homeostasis. *Cell* **159**, 1433–1446 (2014).
75. S. Taheri-Araghi, S. D. Brown, J. T. Sauls, D. B. McIntosh, S. Jun, Single-cell physiology. *Annu. Rev. Biophys.* **44**, 123–142 (2015).
76. C. Droin, E. R. Paquet, F. Naef, Low-dimensional dynamics of two coupled biological oscillators. *Nat. Phys.* **15**, 1086–1094 (2019).
77. C. Feillet, P. Krusche, F. Tamanini, R. Janssens, M. J. Downey, P. Martin, M. Teboul, S. Saito, F. A. Levi, T. Bretschneider, B. van der Horst, F. Delaunay, D. A. Rand, Phase locking and multiple oscillating attractors for the coupled mammalian clock and cell cycle. *Proc. Natl. Acad. Sci. U.S.A.* **111**, 9828 (2014).
78. J. Bieler, R. Cannavo, K. Gustafson, C. Gobet, D. Gatfield, F. Naef, Robust synchronization of coupled circadian and cell cycle oscillators in single mammalian cells. *Mol. Syst. Biol.* **10**, 739 (2014).

Acknowledgments: We are grateful to N. Kleckner for useful feedback on our work and to P. Levin, J. Elf, and P. Nghe for useful discussions. **Funding:** M.C.L. was supported by Associazione Italiana per la Ricerca sul Cancro, AIRC IG grant no. 23258. **Author contributions:** Conceptualization: M.C.L., B.S.; Methodology: I.I., M.C.L., B.S.; Experiments: I.I., G.M., B.S.; Data analysis: I.I., M.C.L.; Funding acquisition: M.C.L., B.S.; Project administration: B.S.; Supervision: M.C.L., B.S.; Writing original draft: I.I., M.C.L., B.S.; Writing review and editing: M.C.L., B.S. **Competing interests:** The authors declare that they have no competing interests. **Data and materials availability:** Datasets of segmented and tracked cells, together with example code for data analysis, were made available through the Mendeley Data Repository DOI: 10.17632/hhp6g5zt8j.1, accessible at the website https://data.mendeley.com/datasets/hhp6g5zt8j/1. All data needed to evaluate the conclusions in the paper are present in the paper and/or the Supplementary Materials.

Submitted 7 February 2024
Accepted 10 June 2024
Published 17 July 2024
10.1126/sciadv.ado5398